Irradiation in BCC materials: Defect-induced changes of the effective dislocation mobility and their relation with the dose-dependent fracture response

Singh Kulbir, Christian Robertson, A.K. Bhaduri

Irradiation in BCC materials: Defect-induced changes of the effective dislocation mobility and their relation with the dose-dependent fracture response

Kulbir Singh *[1], C. Robertson[2] and A.K. Bhaduri[1]

[1]Indira Gandhi Centre for Atomic Research, HBNI, Kalpakkam, India 603 102
[2]DEN-Service de Recherches Metallurgiques Appliquees, CEA, Universite Paris-Saclay, Gif-sur-Yvette, France

Abstract

The mechanical response of nuclear structural materials and their lifetime are strongly affected by radiation effects. This influence is of concern, especially in body centered cubic (BCC) materials, which exhibiting a well-defined ductile to brittle transition. The ductile to brittle transition temperature (DBTT) itself is dose-dependent and may rise to or above the room temperature. In current work, the irradiation effect is modeled to predict the dose-dependent changes of the effective dislocation mobility, represented by the Defect Induced Apparent Temperature Shift (ΔDIAT). Mainly dislocation based crystal plasticity material model is used rather than a phenomenological approach. This material model accounts for both thermally activated dislocation mobility and dislocation mobility in an athermal regime of BCC materials. The defect-induced evolution of ΔDIAT in turn analyzed and their relations with the fracture response are highlighted and bdiscussed.

1 Introduction

In spite of having good thermal properties and excellent resistance to helium embrittlement along with void swelling [1, 2] up to higher dpa (displacement per atom) levels, ferritic and ferritic-martensitic steels are not used extensively for in-core materials due to the concern of irradiation-induced loss of impact strength and fracture toughness along with the rise in DBTT. However, these materials otherwise are considered to be promising for future nuclear reactors [3–5]. Crystal structure (FCC & BCC) governs dislocation mobility, which is the primary reason for such different characteristics of austenitic and ferritic steels. To study such behavior, crystal plasticity models based on the constitutive framework at a level of slip systems within finite element simulations have become an essential tool for material development and continuum mechanics [6, 7].

Dislocation mobility is a fundamental property that determines the plastic deformation in crystals [8–10]. Accordingly, many dislocation based crystal plasticity material models are developed, especially for FCC materials. It is because of their well-known slip system and thermally independent dislocation mobility as contrary to BCC materials. A higher value of Peierls's barrier ($\sim 1GPa$) in BCC materials leads to the strong temperature dependence of dislocation mobility [11–14]. Thermally activated phenomenon viz. kink pair nucleation, assists in dislocation mobility and in turn low temperature plasticity behavior in BCC materials. Hence, a material model should be capable of accounting for temperature dependent plasticity in BCC materials. The crystal plasticity models were developed to investigate the plasticity in BCC materials by Zerilli et al. [15], Armstrong et al. [16], Kubin et al. [14], Stainier et al. [17], Ma et

*Corresponding author
Phone: +91 44 27480500 Extn. 21142, Fax: +91 44 27480104
Email: kulbir@igcar.gov.in

al. [18], Alankar et al. [19], Monnet at al. [20] and Cereceda et al. [13] by using the dislocation density as an internal state variable. Also, attempts have been made to account for irradiation effects on the plasticity of BCC materials. Back in 1960, T.H. Blewitt et al. [21] emphasized the type of interactions possible for radiation induced defects in irradiated material viz. source hardening and friction hardening. Irradiation dose and temperature effect on the yield stress of materials have been routinely described using the dispersed barrier hardening model associating the microstructural changes (defect densities) with an increase in yield strength [22]. The cascade-induced source hardening model developed by Singh et al. [23] is based on the stress necessary to free the dislocations from irradiation-induced defect loops. This process enables the pinned dislocations to act as Frank-read sources for dislocation multiplication. Arsenlis et al. [24] studied model for FCC materials, which assumes the irradiation-induced defects as shearable obstacles to mobile dislocations. These defects possess sufficient obstacle strength and impede the dislocation motion akin to forest dislocations. Dislocation multiplication and annihilation mechanisms are considered for dislocation density evolution.

Due to the involvement of considerable time and high cost in carrying out irradiation tests with a not very controlled environment, it would be beneficial in case reliable material models could be developed with available data. In the current work, a dislocation density based crystal plasticity material model for BCC materials is used to account for temperature dependent plasticity in non-irradiated as well as irradiated materials. The radiation induced defects are considered by incorporating strength based defect-dislocation interaction and also their impact on the mobile and total dislocation density. The model is applied to evaluate the defect-induced dislocation velocity field changes, related to an apparent straining temperature shift ΔDIAT. The latter quantity and its relation with the dose-dependent evolution of the fracture response are then highlighted and discussed.

2 Constitutive Model

The two regimes viz. *thermally activated regime and athermal regime* are addressed separately to define dislocation mobility in BCC materials. In thermally activated regime (at low temperature), overall dislocations mobility is controlled by $b = \frac{1}{2}\langle 111 \rangle$ screw dislocations gliding on the closed-packed crystallographic planes $\{110\}, \{123\}$ and $\{112\}$ (for current work only $\{110\}$ plane is considered). Gliding dislocations have to overcome an energy barrier (also called *Peierls barrier*) characterizing the lattice resistance. Local stress (due to externally applied stress) decreases this energy barrier and dislocation moves in case the applied stress increases the local stress up to the critical value called *Peierls stress*. Dislocation mobility rules defined for each regime are discussed in the subsequent section.

2.1 Thermally Activated Regime

In a thermally activated regime, the velocity of dislocation is dependent upon the effective stress and temperature. The temperature dependence arises from the thermally activated process of kink pair nucleation. As the velocity of a screw dislocation is lesser than the velocity of edge dislocation, the overall dislocation mobility is dependent only upon the screw dislocations velocity [25, 26]. The Arrhenius form of the equation accounting for thermal component and having a dependency of activation enthalpy on effective stress is proposed by Kocks et al. [27]. Based on a similar approach, various dislocation mobility laws are used in the literature [25, 28–30] at a mesoscopic and continuum scale. In current work, the dislocation velocity for the thermal regime is defined based on the following relationship:

$$v = \frac{\nu_d b h}{L_c^2} exp\left[-\frac{\Delta H_0}{k_B T}\left(1 - \left[\frac{\tau_{eff}}{\tau_0}\right]^p\right)^q \right] l_s \tag{1}$$

where ν_d is Debye frequency, b is the magnitude of Burger's vector, h is the distance between Peierls valleys, L_c is the critical length of kink pair, ΔH_0 is a kink pair activation enthalpy at $0K$, k_B is Boltzmann constant, T is absolute temperature, τ_{eff} is effective resolved shear stress on slip plane, τ_0 is Peierls shear stress at $0K$, l_s is the average length of the screw dislocation segment and p & q are constants.

The stress (τ_{eff}) dependency of L_c ($= \sqrt{(\mu bh)/(8\pi\tau_{eff})}$, discussed in section 2.3) and v_d is used to express the dislocation velocity v as:

$$v = \frac{8\pi\tau_{eff}^2}{\mu B} exp\left[-\frac{\Delta H_0}{k_B T}\left(1 - \left[\frac{\tau_{eff}}{\tau_0}\right]^p\right)^q\right] l_s \tag{2}$$

where μ is the shear modulus and B is the viscous drag coefficient.

The stress dependent pre-factor in Eq. 2 accounts for having several kink pair nucleations taking place with temperature increase as L_c is stress dependent. It leads to a gradual transition within the thermal regime towards the athermal regime. Whereas, stress independent pre-factor (constant value) assumes single kink pair nucleation is responsible for the movement of screw dislocation from one Peierls valley to next, which is valid only for very low temperature range (up to $100K$).

Further, using classical Orowan's relation to relate mobile dislocation density (ρ_m), velocity (v) with strain rate ($\dot{\gamma}$) as $\dot{\gamma} = \rho_m b v$, strain rate for this regime is expressed as:

$$\dot{\gamma}_{Thermal} = \rho_m b \frac{8\pi\tau_{eff}^2}{\mu B} exp\left[-\frac{\Delta H_0}{k_B T}\left(1 - \left[\frac{\tau_{eff}}{\tau_0}\right]^p\right)^q\right] l_s \tag{3}$$

Eq. 3 gives the strain rate dependence upon temperature (T), effective resolved shear stress (τ_{eff}), and the average length of screw dislocation segment (l_s).

2.2 Athermal Regime

In the athermal regime, the mobility of dislocations is only dependent upon the effective resolved shear stress (τ_{eff}) since it is controlled by the edge dislocation velocity ($v_{edge} = \tau_{eff} b/B$). The presence of thermally activated jog drag in the dislocation induces minor thermal component at the macroscopic scale in flow-rule. For this regime, the strain rate is expressed as a classical viscoplastic potential, based on the applied resolved shear stress (τ_{RSS}) and critical shear stress τ_c as:

$$\dot{\gamma}_{Athermal} = \dot{\gamma}_0 \left(\frac{\tau_{RSS}}{\tau_c}\right)^n \tag{4}$$

where $\dot{\gamma}_0$ is reference shear strain rate, and n is constant. This equation represents the Arrhenius equation rewritten in the power-law form [31], which is routinely used in crystal plasticity material models to address the athermal regime. This constitutive equation has numerical limitations due to the very high value of n (≥ 100). Generally, a lower value of n (≤ 50) is used for adaptation of this law in crystal plasticity, which may add the macroscopically incompatible response of rate sensitive evolution. The dislocation length term l_s in Eq. 3 may need revision to represent the athermal regime more accurately. Such new development and implementation would also benefit in direct comparison with *Dislocation Dynamics* (DD) simulation results, using similar stress-velocity rules [30, 32].

The flow-rules discussed in section 2.1 and 2.2 are for very low temperature (affected by thermal fluctuations) and athermal temperature (independent of the thermal fluctuations), respectively. At intermediate temperature values, the two mechanisms should lead to strain rate having a combined effect against the applied load. At these temperature values, total time comprises of time spent by dislocation for kink pair nucleation-propagation (thermal regime) and time spent by dislocation whose mobility is governed by jog drag (athermal regime). Total time taken by dislocation to move could be expressed as the sum of $t_{Thermal}$ and $t_{Athermal}$. The strain rates $\dot{\gamma}_{Thermal}$ and $\dot{\gamma}_{Athermal}$ are inversely proportional to the time spent in their respective regimes; this leads to the following expression for the total strain rate due to both mechanisms.

$$\frac{1}{\dot{\gamma}_{total}} = \frac{1}{\dot{\gamma}_{Thermal}} + \frac{1}{\dot{\gamma}_{Athermal}} \tag{5}$$

This expression implies the smooth transition from a thermally activated regime to the athermal regime. At low temperature, the term $\dot{\gamma}_{Thermal} \ll \dot{\gamma}_{Athermal}$ as effective stress value is high, which leads to total strain rate $\dot{\gamma}_{total}$ equal to $\dot{\gamma}_{Thermal}$. Whereas, at high temperature values (i.e., athermal regime) the $\dot{\gamma}_{Athermal} \ll \dot{\gamma}_{Thermal}$ because of low effective stress and hence, the plastic flow is controlled by $\dot{\gamma}_{Athermal}$. It is worth mentioning that the stress dependent pre-factor used in Eq. 3 helps in the gradual transition between the thermal and athermal regime.

2.3 Screw Segment Average Length And Obstacle Strengthening

The dependence of screw dislocation velocity on its length is supported by an experimental work carried out by Caillard [33] and subsequently introduced in molecular & dislocation dynamics models [25, 28, 34]. The distance between forest obstacles encountered by the screw dislocations governs the average length of the screw dislocation segment, especially at low temperatures. In the absence of obstacles, screw dislocation at low temperature move as a straight line with a single kink pair. However, it no longer remains straight in case it has to pass through obstacles. It is evident from experiments carried out on single crystal niobium at low temperature [35] and mesoscopic scale simulations [14, 36] that two non-screw sections form whenever the screw dislocation encounters an obstacle. The non-screw segment bows out and form the curved shape of radius R_s under the effect of line tension. Assuming dislocation as an elastic string with constant energy per unit length, a simple line tension model gives the value of the radius of curvature as $R_s = \mu b/2\tau_{eff}$ [37]. Such interaction of screw dislocation with an obstacle is characterized by the critical breaking angle ϕ_c, which is an angle that dislocation makes around the obstacle when it breaks. Depending upon the spacing between obstacles, dislocations can by-pass the obstacle in different configurations [20, 29]. Average obstacle strength is estimated based on the type, number, and strength of the individual obstacles present in microstructure [29] and defined as:

$$\alpha^A = \sqrt{\sum \alpha^{AF} \frac{\rho^F}{\rho^A_{obs}}} \tag{6}$$

where α^A is average obstacle strength for activated slip system, α^{AF} is the interaction coefficient between activated slip system A and the obstacle family F, ρ^F is the obstacle density of F and ρ^A_{obs} is total obstacle density for activated slip system. The initial value of ρ^A_{obs} is equal to the dislocation density on the activated slip system, whereas the ρ^F is taken as a sum of dislocations on the rest of the slip systems.

To calculate the screw segments average length, first average obstacles spacing (λ) is estimated depending upon the average obstacles size D. The estimation of term λ is adapted from the work of G. Monnet et al. [29] which is based on isotropic dislocation mobility (in athermal regime) and anisotropic dislocation mobility (in thermally activated regime) [36]. The general expression for the estimation of λ in all regimes is:

$$\lambda = \frac{1}{min[\sqrt{\rho^A_{obs}}; (2R_s + D)\rho^A_{obs}]} - D \tag{7}$$

Using the geometric relation between average obstacles spacing and radius of curvature (dependent on critical radius and obstacle strength), the average length of the screw segments is expressed as:

$$l_s = max[\lambda - 2\alpha^A R_s; l_{lim}] \tag{8}$$

α is the strength coefficient. l_{lim} is limiting the value of the average length of screw dislocations calculated based on L_c value. A constant value of L_c is assumed by Tang et al. [25], whereas it is taken as temperature dependent by Monnet et al. [29]. In present work, since temperature and irradiation effects are studied, an effective shear stress dependent value of L_c is considered, and the same is expressed as:

$$L_c = \sqrt{\frac{\mu b h}{8\pi\tau_{eff}}} \tag{9}$$

Based on the above expression l_{lim} is defined as $f_c \times L_c$, where f_c is constant, its value is estimated from experimental results of pure iron for activation volume reported in the literature [38–40].

2.4 Effective Shear Stress

Only resolved shear stress (τ_{RSS}) acting on the glide plane and in the slip direction produces a glide force on a dislocation. The slip system with the highest resolved shear stress acting upon it predominates in the slip process [41]. The τ_{RSS} provides the driving force for dislocation mobility, but there is always some resistance to dislocation mobility. The shear stress must reach a critical value called *critical resolved shear stress* (τ_c) for moving dislocation. Hence, the effective shear stress τ_{eff} which is the stress required to impart velocity v to the screw dislocation segment and can be expressed as $\tau_{eff} = |\tau_{RSS}| - \tau_c$ (τ_c comprises of all the resistance to the dislocation glide). In the present model, τ_c is defined [29] as:

$$\tau_c = \sqrt{\tau_{self}^2 + \tau_{LT}^2} \tag{10}$$

Stress due to an interaction between all dislocations present on the same slip system (τ_{self}) is calculated like forest hardening rule having strength coefficient between same slip system (α_{self}) as $\tau_{self} = \mu b\sqrt{\alpha_{self}\rho^A}$.

The line tension resistance on dislocations (τ_{LT}) contributes in case of smaller spacing between obstacles [20]. In such a case, there is a requirement of a decrease in radius of curvature before dislocation can unpin from the obstacle. This leads to line tension resistance corresponding to $\tau_{LT} = \tau_{R_c} - \tau_R$ expressed as:

$$\tau_{LT} = \frac{\mu b}{2R_C} - \frac{\mu b}{2R} \tag{11}$$

with $R_c = \lambda/2\alpha$, here α depends upon the forest dislocation density and corresponding strength of the interaction.

The relative strength between each slip system is predicted by adapting the matrix form of the above relation with dimensionless interaction matrix $[\alpha^{AF}]$ [19, 42–48]. Here $[\alpha^{AF}]$ is the interaction matrix of a size equivalent to the number of interacting slip systems considered, and its coefficients represent the corresponding strengths of the interaction. For current simulation's temperature range, 12 slip systems (size $[\alpha^{AF}] = 12 \times 12$) are adequate as other 24 system participates significantly at the higher temperature ranges (above 400 K). Further, due to symmetry, six independent coefficients are sufficient to define the interaction matrix [46]. With recent advances in DD simulations, the interaction matrix coefficient can be estimated [49, 50] with enough accuracy.

2.5 Dislocation Density Evolution

The dislocation density (ρ) evolution for any slip system is fully controlled by two oppositely acting phenomena viz. storage and annihilation of dislocations. These two phenomena are dependent upon the strain & dislocation density values and are related as $d\rho/d\gamma = k_1\rho^{1/2} - k_2\rho$; the first term represents storage, and the second term represents the annihilation of dislocations [31]. The storage term is responsible for the increase in flow stress with strain and can be expressed using dislocations mean free path Λ, whereas annihilation term responsible for dynamic recovery and depends linearly on dislocation density. The Λ is a distance traveled by a dislocation segment before it is stored by interaction with the microstructure. The final expression for dislocation density evolution as a function of strain can be written as [51, 52]:

$$\frac{d\rho}{d\gamma} = \frac{1}{b}\left[\frac{1}{\Lambda} - y\rho\right] \tag{12}$$

y is a material parameter that accounts for dynamic recovery, and Λ accounts for dislocation storage.

The contribution to the mean free paths arises from the interactions of moving dislocations with forest dislocations, along with interaction within the same slip system and their subsequent storage. Work carried by Devincre et al. [52] proposed the mean free path estimation methodology. This approach is

subsequently adapted by Monnet et al. in reference [29] to give the following expression (representing activated slip system) for Λ, and the same is adopted in this work:

$$\frac{1}{\Lambda} = \left(1 - \frac{\tau_{eff}}{\tau_0}\right) \frac{\sqrt{\alpha_{self}\rho^A}}{K_{self}} + \frac{\alpha^A \lambda^A \rho^A_{obs}}{K_{forest}} \tag{13}$$

The annihilation term ($y\rho^A$) is responsible for dynamic recovery in the material and has a dependence on temperature. In this term, y is the dynamic recovery parameter proportional to the critical annihilation distance of dislocations by cross slip [52]. Value of y is defined by using a harmonic average of critical distance in thermal and athermal regime to account for temperature dependence [29]:

$$\frac{1}{y} = \frac{1}{y_{Athermal}} + \frac{2\pi\tau_{eff}}{\mu b} \tag{14}$$

where $y_{Athermal}$ is the critical annihilation distance in the athermal regime. The second (τ_{eff} dependent) term controls the y value at low temperature. Based on the temperature value, the two terms contribute to the net value of y.

3 Irradiation Hardening Modeling

Unlike FCC materials, BCC materials exhibit DBTT in the temperature range of 0 and $300K$. This is mainly attributed to the temperature dependent dislocation mobility in BCC materials as compared to athermal mobility in FCC materials. In the presence of irradiation, ferritic materials harden with a reduction in ductility and most importantly, rise in DBTT [1, 2, 53]. An interaction between neutrons and lattice atoms induces primary knocked atom displacements and subsequently, radiation damage in crystalline materials: in the form of defect dispersion, including interstitial dislocation loops [54].

The dislocation being a primary carrier of the plasticity in crystalline materials, the interaction of dislocation with other dislocations, irradiation-induced defects, precipitates, point defects, and surface defects, etc. may lead to change in the dislocation velocity field and eventually lead to strain localization. The relative dislocation mobility alteration due to such interactions could be utilized as a basis to study the changes in material behavior due to the presence of such defects to no defect condition. Molecular dynamics simulation carried out by Terentyev et al. [55] shows that the interaction of dislocation loop (irradiation defect) with screw dislocation leads to the loop absorption by mobile dislocations in the form of helical jogs. In BCC-Fe materials, helical jogs are mostly unstable and hence, tends to collapse by emitting a new prismatic loop after unpinning completes at the displaced position. An edge-loop interaction is comparatively weaker than screw-loop interaction, and also due to edge-loop interaction, loops are neither damaged nor displaced after the completion of their interaction [56].

In present work, the emphasis is given on defect dispersions produced due to irradiation (dislocation loops) to account for radiation effects. In subsequent subsections, evolution laws for irradiation defect density and mobile dislocation density considered in the model during material straining are discussed.

3.1 Irradiation Defect Density

A high number of defects in the form of interstitial loops are produced during high temperature (300-500 °C) irradiations [57]. Back to room temperature, loops are mostly stable and immobile with respect to strain-induced dislocations [58]. These loops restrict the motion of the mobile dislocations and thus produce irradiation hardening, which increases the yield strength and decreases the ductility. To account for the irradiation loops effect at the continuum scale, they are modeled as obstacles (with their strength value) to the mobility of the dislocations. Irradiation defects are assumed to be uniformly dispersed in the material.
Irradiation loops are treated as obstacles with density $\rho_{irr} = N_{irr} d_{irr}$ and average strength α_{irr} present on all slip systems. The average loop strength is predicted (~ 0.3) by DD investigations of sub-grain

plastic spreading in the presence of defect dispersions, and similar value of α_{irr} is reported by Arsenlis et al. [24]. The N_{irr} is the number density of the loops, and d_{irr} is the average diameter of the loops. Both these parameters are strongly dependent upon the irradiation dose (controls the N_{irr}) and irradiation temperature (controls the d_{irr}).

On an active slip plane, mobile dislocations interaction with irradiation defects leads to a gradual decrease in their number density. After successive screw-loop interactions, the loop is displaced from its initial position. Once this displacement reaches the lath size, the loop ceases to interact with mobile dislocation (see Fig. 1). This phenomenon leads to a reduction in irradiation defect density on the active slip system where adequate screw-loop interactions take place. Nevertheless, the irradiation defect density on other slip systems remains nearly unaltered until these systems become active. The following phenomenological relation, which defines the rate of change of irradiation defect density in terms of strain rate, is adapted to account for this.

$$\dot{\rho}_{irr} = -\xi \rho_{irr} \dot{\gamma} \tag{15}$$

where ξ is the loop annihilation parameter.

The presence of irradiation defects (dislocation loops) augment the number of total obstacles and hence, accounted appropriately to calculate the total obstacle density ρ^{A}_{obs} on activated slip system in the calculation of λ value (Eq. 7) and the average strength of obstacles α^{A} (Eq. 6). The value of ξ is found to be independent of temperature and depends only upon the strain rate as per DD simulation results [58]. An internal state variable corresponding to the respective ρ_{irr} is considered for each slip system.

3.2 Mobile Dislocations Density

The mobile dislocation density (ρ_m) changes marginally in the absence of irradiation defects and hence, assumed to be constant in the model. Whereas in the presence of irradiation, generally dislocations density ρ increases, and also through DD simulation, it is observed that there is a significant increase in mobile dislocations density ρ_m [30]. This increase in ρ_m may be attributed to the interaction of irradiation defects with screw dislocations. On the interaction of the screw dislocation line with the irradiation loop, it forms jogs of size almost equal to the size of the loop (can be smaller in few cases). This creates the pinning of screw dislocations as the jogs (steps) are in a different plane, and the step line has the nature of edge dislocation. These sites subsequently act as a source for mobile dislocations. Whenever the screw dislocation interacts with the irradiation loop, there is a strong possibility for the creation of the mobile dislocation source. As per the DD simulations carried out by Robertson et al. [58] and Gururaj et al. [30] on the interaction of irradiation defects with dislocations, it is observed that 5-10 screw-loop interactions must be there before the dislocation loop moves out of the lath due to a shift in its position after successive interaction (Fig. 1). This phenomenon of formation of dislocation sources and subsequently, the generation of mobile dislocation [23, 24] is incorporated in the current material model. The rate of increase of mobile dislocations due to interaction with irradiation defects is expressed in terms of irradiation defect density change as:

$$\dot{\rho_m} = \frac{\kappa \xi}{r_0} \rho_{irr(t)} \dot{\gamma} \tag{16}$$

where κ is the number of screw-loop interaction produce source before irradiation loop's removal from lath and r_0 is the initial ratio of ρ_{irr} and ρ_m.

4 Defect Induced Apparent Temperature Shift

The dislocation mobility is the governing phenomenon controlling the temperature-dependent evolution of fracture toughness in BCC materials. The dislocations emitted from the crack tip region reduces the

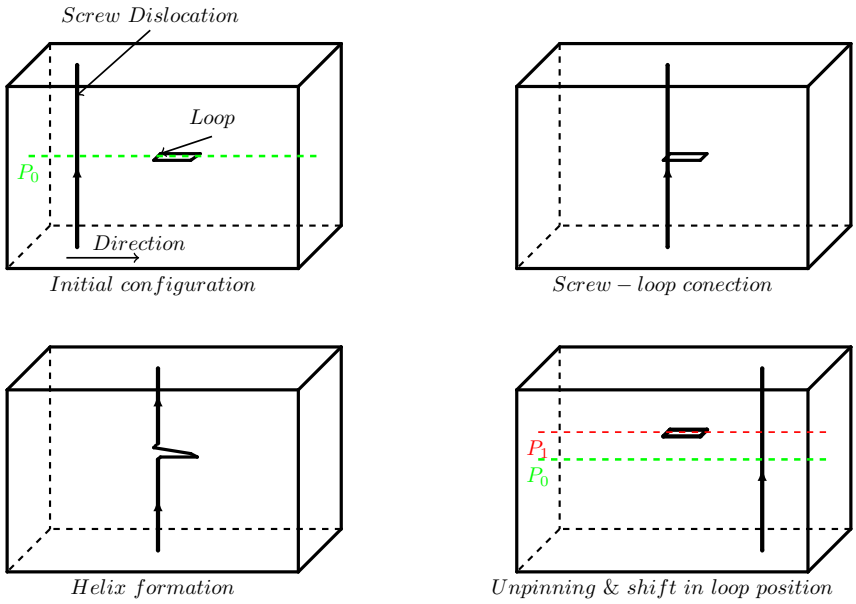

Figure 1: Interaction of screw dislocation with irradiation loop: Shifts irradiation loop (from P_0 to P_1) in direction of $\vec{b}$

stress intensity, therefore, resulting in crack tip blunting [59], this could be mainly attributed to the increase in plastic strain due to dislocation mobility. The materials with lower dislocation mobility would fracture at lower applied stress as compared to the materials having higher dislocation mobility. The DBTT shift is dependent upon various effects acting simultaneously viz. radiation embrittlement, deformation aging, thermal aging, and low-cycle fatigue damage [60]. It is known that the major contribution towards the value of the DBTT shift is imparted by radiation induced defects. In the case of irradiation, due to the presence of the irradiation defects, there is a change in the velocity field of the dislocations which, subsequently leads to a relative reduction in the applied stress to produce fracture. An analogous principle has been used to reckon the effect of irradiation defects on the brittle to ductile transition by Swinburne et al. [61]. It is essential to mention that in the presence of irradiation defects, there is a significant increase in mobile dislocation density, which in turn reduces the v and τ_{eff} values. Figure 2 compares the effect of straining on various mobility parameters in the non-irradiated and irradiated case along with graphical representation on $v - \tau_{eff}$ diagram.

To quantify the effect of irradiation-induced defects on the DBTT, a new concept called Defect Induced Apparent Temperature shift (ΔDIAT) is introduced by Li et al. [32]. The ΔDIAT value provides the quantification of change in behavior of the materials in terms of temperature, which subsequently relates to the DBTT shift due to irradiation. A negative value of the ΔDIAT implies the velocity field of dislocations in the presence of irradiation defects is equivalent to the velocity field in case of no irradiation defects strained at a lower temperature (see Fig. 2). Hence, the ΔDIAT value can be estimated based on the relative change in the velocity field of dislocations. The following relation is derived to find the apparent temperature of irradiation case to predict the ΔDIAT, which is equal to $T_1 - T_0$:

$$\frac{\overline{v_0}}{v_1}\left(\frac{\tau_{eff_1}}{\overline{\tau_{eff_0}}}\right)^{1.5} = exp\left(\frac{\Delta H_{eff_1}}{ck_BT_1} - \frac{\Delta\overline{H_{eff_0}}}{ck_BT_0}\right) \tag{17}$$

subscript '0' represents the non-irradiated case, and '1' represents the irradiated case. In Eq. 17 $\overline{v_0}$, $\overline{\tau_{eff_0}}$ are the average value of dislocation velocity & effective shear stress in the non-irradiated case, and $\Delta\overline{H_{eff_0}}$ is the average value of effective enthalpy. Effective enthalpy is related to ΔH_0 with relation $\Delta H_{eff} = H_0\left(1 - \left[\frac{\tau_{eff}}{\tau_0}\right]^p\right)^q$. c is constant with value lying between 1 and 2 depending upon the dominance of the thermal or athermal regime, respectively. Knowing the velocity and effective shear stress of non-irradiated case at the temperature T_0, apparent temperature T_1 equivalent to temperature having the same

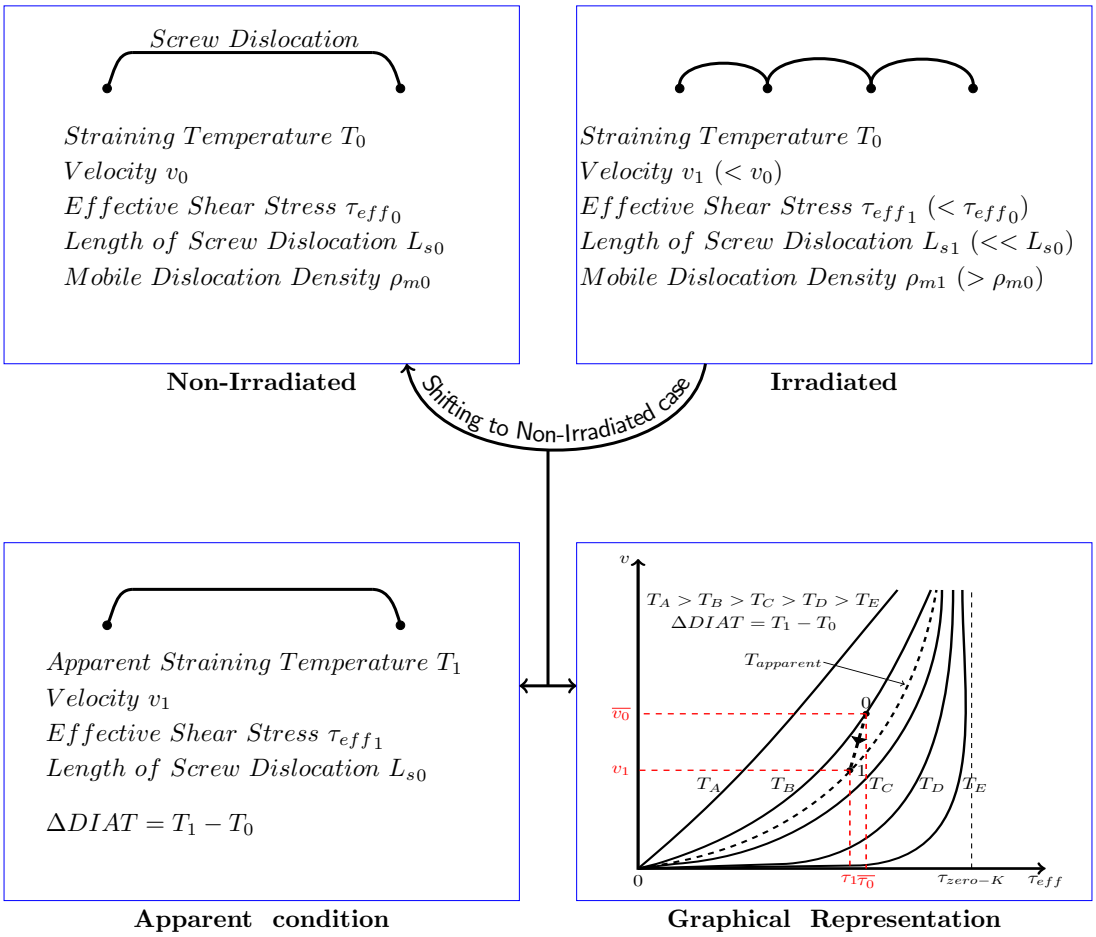

Figure 2: ΔDIAT concept schematic and graphical representation on a typical $v - \tau_{eff}$ plot.

velocity field as in irradiated case is estimated.

5 Finite Element Modeling And Validation

The dislocation based material model with constitutive equations discussed in the previous sections is implemented using *mfront* [62], an open-source code. Subsequently, the behavior under applied load is predicted using the finite element method (FEM) with a finite deformation framework. The local deformation gradient tensor (F) is decomposed into elastic (F^e) and plastic (F^p) gradients related through relation $F = F^e F^p$ [18, 63, 64]. Here, F^p represents the deformation due to plastic shearing on crystallographic slip systems, and F^e represents the rotation and stretching/elastic deformation part.

The FEM is used to simulate tension up to 10% global strain at a constant strain rate of $10^{-4}s^{-1}$ for a single-crystalline beam with dimensions of $10 \times 10 \times 200$ micron. The material orientation is taken such that crystallographic direction $[\bar{1}49]$ of BCC crystal is aligned with the loading axis as this direction is close to the center of the standard triangle of stereographic projections, this ensures a single slip during initial loading. The loading and boundary conditions are shown schematically in Fig. 3.
The values of various material parameters used in the material model are listed in Table 1. In the current work, elastic behavior is considered to be isotropic.

For the material model validation, results are compared with an experimental work carried out in terms of critical resolved shear stress [38–40] on pure iron crystal, shown in Fig. 4. The numerical simulation results are found to be in good agreement with experimental results (with an initial dislocation density value 5×10^{11} m^{-2}) and exhibits the capability of the material model in addressing both thermal and

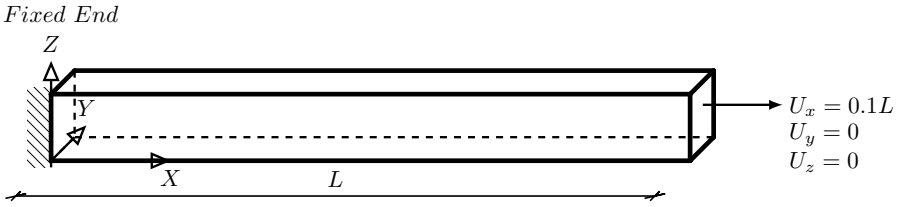

Figure 3: Schematic representation of loading and boundary conditions

Table 1: Material parameters [29, 30]

Parameter	Value/function	Units	Parameter	Value/function	Units
b	0.2481	nm	p	0.593	-
E	$236.4-0.0459T$	GPa	q	1.223	-
ν	0.35	-	D	10	nm
ΔH_0	0.76	eV	$y_{Athermal}$	2	nm
τ_0	360	MPa	$\rho^{initial}$	4×10^{12}	m^{-2}
$\dot{\gamma}_0$	1.0E-6	s^{-1}	$\rho_{irr}^{initial}$	50×10^{12}	m^{-2}
n	50	-	α_{irr}	0.3	-
B	10.5×10^{-11}	$MPa.s^{-1}$	ξ	4	-
f_c	6	-	κ	4	-
k_B	8.6173×10^{-5}	eV/K	c	1-2	-
$\alpha^{AF}{}_{coll.}$	0.7	-	$\alpha^{AF}{}_{non-coll.}$	0.1	-
K_{self}	100	-	K_{forest}	$\frac{K_{self}}{min(3,1+\frac{2}{300}T)}$	-

athermal regimes.

6 Simulation Results

The numerical simulations on beam case are carried out at different temperature values within a range of 100 K to 350 K for the non-irradiated and irradiated cases. The results shown for irradiated case in the subsequent section corresponds to the irradiation condition for the loop size of 5 nm (Irradiation temperature $(T_{irr}) > 70^{\circ}C$) with irradiation defect cluster density value as $10\times10^{21}\ loops/m^3$.

6.1 Non-Irradiated Case Results

The variation of total dislocations density (ρ_{tot} *or* ρ^A) on the primary slip system for various temperatures with respect to strain on the primary slip system (ε_{pss}) is shown in Fig. 5a. The value of ρ_{tot} increases with an increase in temperature and applied strain. The direct dependence of τ_{self} upon the ρ_{tot} value is evident from Fig. 5b in which τ_{self} follows a similar variation in terms of temperature and strain as of ρ_{tot}. The τ_{LT} contribution is negligible at low temperatures, starts participating when l_s reaches its limiting value of l_{lim}, this is possible at higher temperatures (mainly due to higher dislocation density

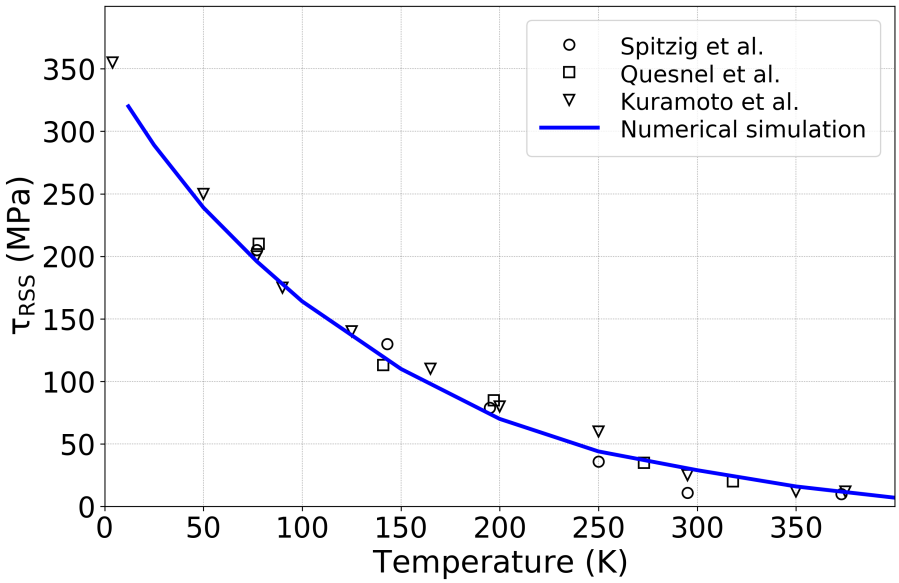

Figure 4: Validation of material model with experimental results reported by Spitzig et al. [38], Quesnel et al. [39] and Kuramoto et al. [40] against critical resolved shear stress.

and reduction in the effective shear stress). The temperature dependent variation of τ_{LT} with strain is shown in Fig. 6a.

The values of shear stresses, τ_c, τ_{eff}, and τ_{RSS} corresponding to the 5% plastic strain on the primary slip system are shown (Fig. 6b) as the function of temperature (strain dependency of these stresses is negligible). Up to 250 K, the value of τ_c is only governed by τ_{self} (contribution of τ_{LT} is small) and increases marginally (< 4 MPa) with an increase in temperature. Once the τ_{LT} begins to contribute (after 250 K), the value of τ_c starts increasing and finally leads to a significant decrease in applied shear stress (τ_{RSS}) reduction rate with temperature.

6.2 Irradiated Case Results

The numerical simulations are carried out for the irradiated case with the material model discussed in the previous section (Sec. 3). The irradiation temperature is considered in total irradiation defect density value by size term d_{irr}. The evolutions of various parameters on the primary slip system for irradiation case are shown in Fig. 7. The following are the major observations in comparison to the non-irradiated case:

- The evolution of ρ_{tot} shown in Fig. 7a highlights the increase in total dislocation density value and shifting total dislocations evolution with strain from almost linear to non-linear variation as compared to the non-irradiated case (Fig. 5a).
- The increased value of dislocation density leads to an increase in τ_{self} (shown in Fig. 7b) as compared to the non-irradiated case (Fig. 5b).
- In the case of τ_{LT} (shown in 8a), its contribution to internal stress starts from a lower temperature; this is mainly due to the presence of more obstacles (forest dislocations and irradiation defects). It is essential to highlight that the evolution of τ_{LT} in terms of straining is opposite to the non-irradiation case (Fig. 6a); this is because of the annihilation of irradiation defects with straining.
- The variation of τ_c, τ_{eff}, and τ_{RSS} at 5 % strain is shown in Fig. 8b. The higher value of τ_{self}, a significant contribution of τ_{LT} from lower temperature range and their higher magnitude leads to a substantial rise in the applied shear stress τ_{RSS} value as compared to the non-irradiation case (Fig.

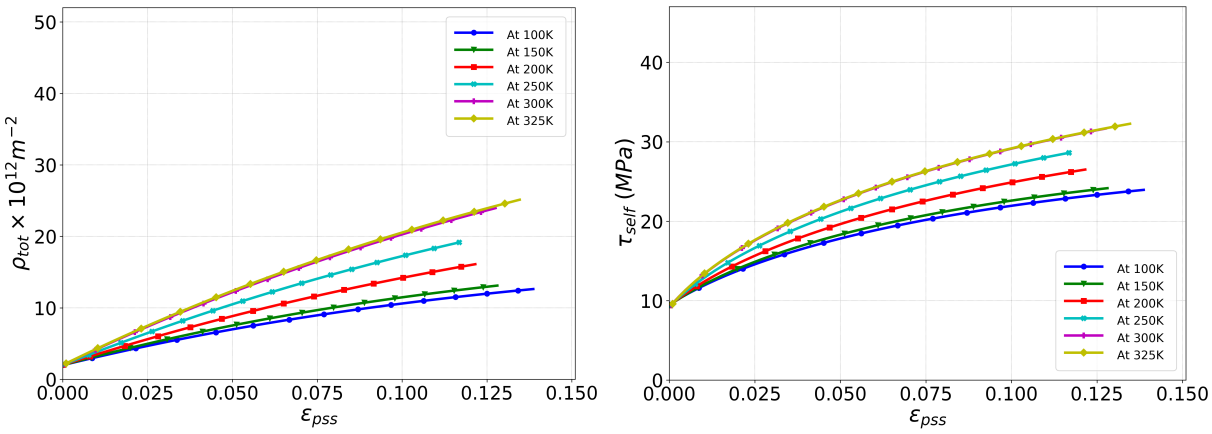

(a) (b)

Figure 5: Numerical simulation results for the non-irradiated case, a) Total dislocation density as a function of strain on the primary slip system, b) Self interaction stress on the primary slip system.

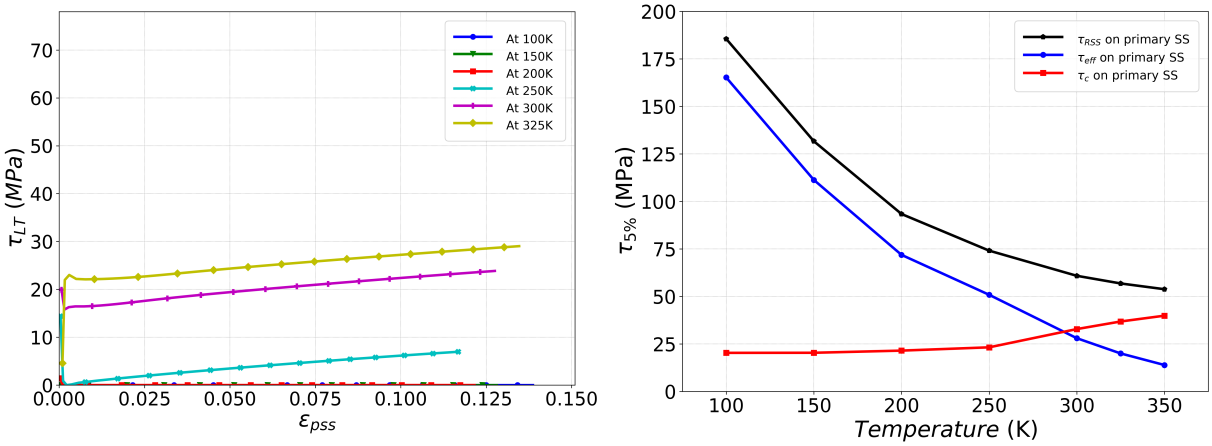

(a) (b)

Figure 6: Evolution of a) line tension component of shear stress and b) Temperature dependency of shear stresses (τ_c, τ_{eff} and τ_{RSS}) on primary slip system (SS) at 5% strain (Non-irradiated case).

6b). It is evident from Fig. 8b that the numerical model is predicting an effect of irradiation hardening satisfactorily, which leads to an increase in yield point as compared to the non-irradiation case.

- The reduction in ρ_{irr} with straining is due to continuous interaction between dislocation and irradiation defects (shown in Fig. 9a). The annihilation of irradiation defects is considered to be athermal.

- The value of ρ_m increases in-line with the annihilation of irradiation defects (see Fig. 9b). The strain localization on a single slip system leads to higher net annihilation of irradiation defects and correspondingly reduction in the rate of increase of ρ_m values.

The value of the average length of screw dislocation (l_s) for non-irradiated case decreases with an increase in temperature and straining due to dislocations multiplication (Fig. 10a). At a higher temperature range, the value of l_s is governed by l_{lim}, which remains nearly constant for specific temperature since it is only dependent upon τ_{eff}. In the irradiated case, the presence of a large number of irradiation defects hinders the motion of dislocations. Consequently, the average length of a screw dislocation is smaller in contrast to the non-irradiated case (Fig. 10*a*) for all temperature ranges. It is interesting to

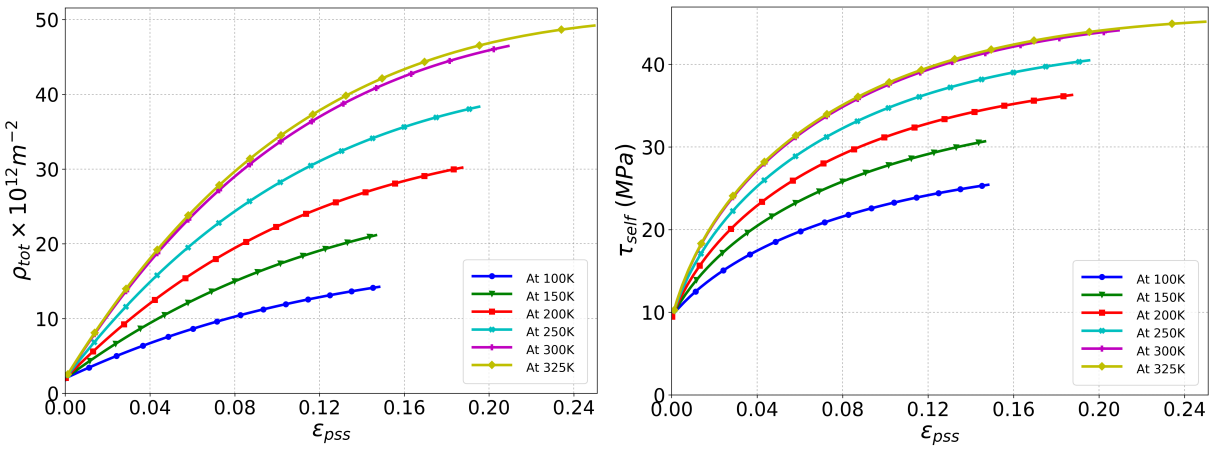

(a) (b)

Figure 7: Numerical simulation results for the irradiated case, a) Total dislocation density, b) Self interaction stress of dislocations.

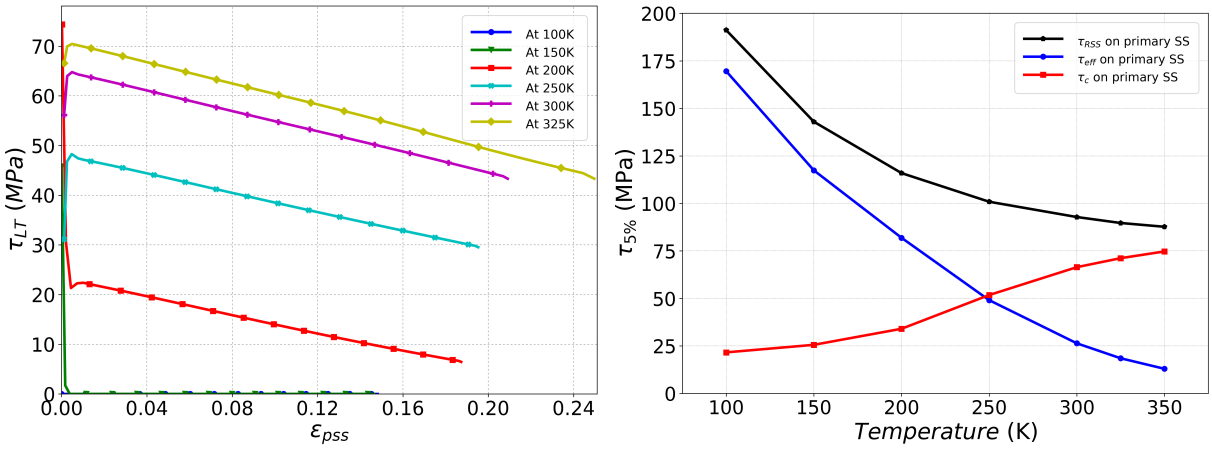

(a) (b)

Figure 8: Numerical simulation results for the irradiated case, a) Line tension stress component and b) Temperature dependency of shear stresses (τ_c, τ_{eff} and τ_{RSS}) on the primary slip system (SS) at 5% strain (Irradiated case).

observe that the value of l_s decreases with straining for the non-irradiated material, whereas it increases in the case of irradiated material. For the non-irradiation case, a decrease in l_s is due to the continuous increase of obstacles present in the form of forest dislocations due to straining. For irradiated material, the annihilation of irradiation defects dominates over the rise in the forest dislocations. This leads to a reduction in an overall number of obstacles with straining and hence, an increase in l_s value is observed.

Figure 10b shows the variation of screw dislocation velocity $v = \dot{\gamma}_{total}/\rho_m b$ on the primary slip system. In the non-irradiated case, ρ_m is taken as constant, hence the variation of velocity is mainly due to the sharing of strain within various slip systems. The primary slip system at 100 K and 325 K have a higher velocity. Hence they share more strain compared to other temperature cases, especially at an intermediate temperature range of 200 K and 250 K. In the case of irradiated material, the value of screw dislocation velocity reduces due to increasing ρ_m value. It is also observed from the results that near the final stage of the deformation, there is regain in the velocity of dislocation (above 200 K) (see Fig. 10b). Significant strain localization at higher temperature range induces the saturation in ρ_m value after a certain amount of straining; subsequently, it needs to regain the dislocation velocity to comply with imposed deforma-

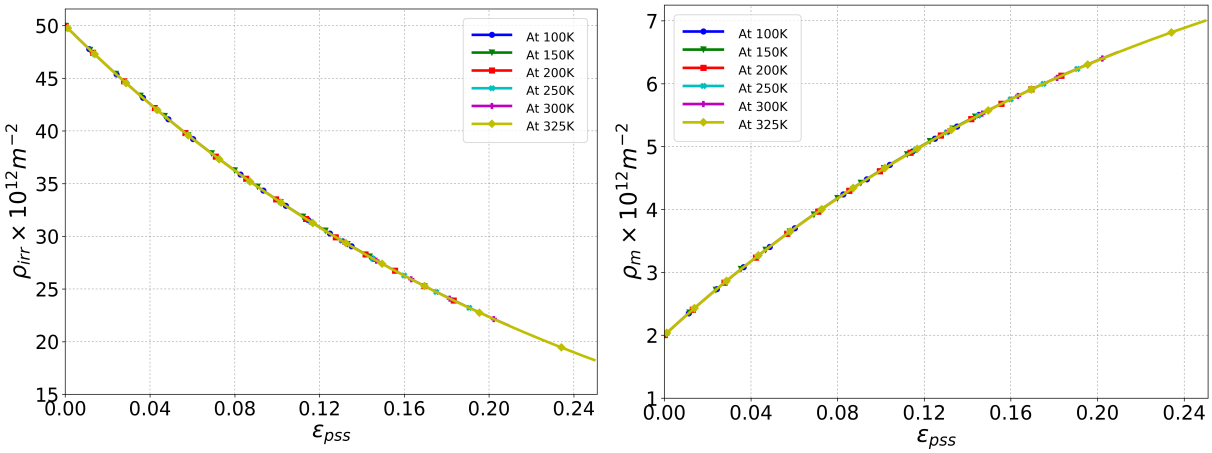

(a) (b)

Figure 9: Numerical simulation results for a) Irradiation defect density and b) Mobile dislocation density evolution; against the strain on primary slip system

tion loading requirements. The imposed strain (global) is not shared among the non-primary slip planes in irradiated material (due to strain localization), which is not in the non-irradiated case where significant participation of non-primary slip planes is observed. Stronger the strain localization more would be the regain in the velocity. The annihilation of irradiation defects by sliding dislocations, formation of defect-free channels, and formation of micro-voids and cracks are major phenomenons during the plastic deformation of irradiated materials. These defect-free channels provide the regions where the dislocation slip is easy, establishing the highly localized plastic deformation zone. The plastic deformation is observed to be concentrated mainly within these cleared channels and is responsible for the observed loss of ductility; this is also observed experimentally [65–68]. The formation of defect-free channels would subsequently lead to strain softening (maintaining higher stress level) at the local level in the material. [69, 70]. An increase in velocity signifies strain-softening after strain localization happening locally in the material.

Based on the results of the non-irradiated case and irradiated case in terms of the effect on the dislocation velocity field, the value of ΔDIAT is estimated using Eq. 17. The ΔDIAT provides a direct estimate of the shift in DBTT due to irradiation defects. In addition to the estimation of ΔDIAT for the loop size of 5 nm with irradiation defect cluster density of 10×10^{21} $loops/m^3$ (0.01 dpa), also the case of irradiation defect cluster density 2×10^{21} $loops/m^3$ and 30×10^{21} $loops/m^3$ (for 5 nm dia) corresponding to 0.002 dpa and 0.15 dpa respectively [71, 72] are studied. The ΔDIAT shift is estimated for these irradiation dose conditions at straining temperatures ranging from 250 K to 350 K (Fig. 11).

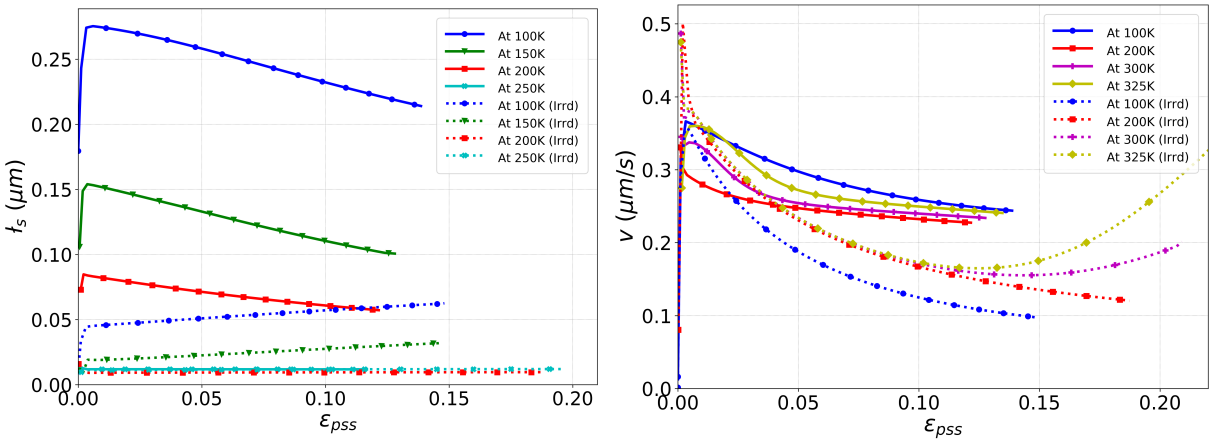

(a) (b)

Figure 10: Comparison of the non-irradiated case (solid line) and irradiated case (dotted line) in terms of a) The average length of screw dislocation and b) The average screw dislocation velocity on the primary slip system.

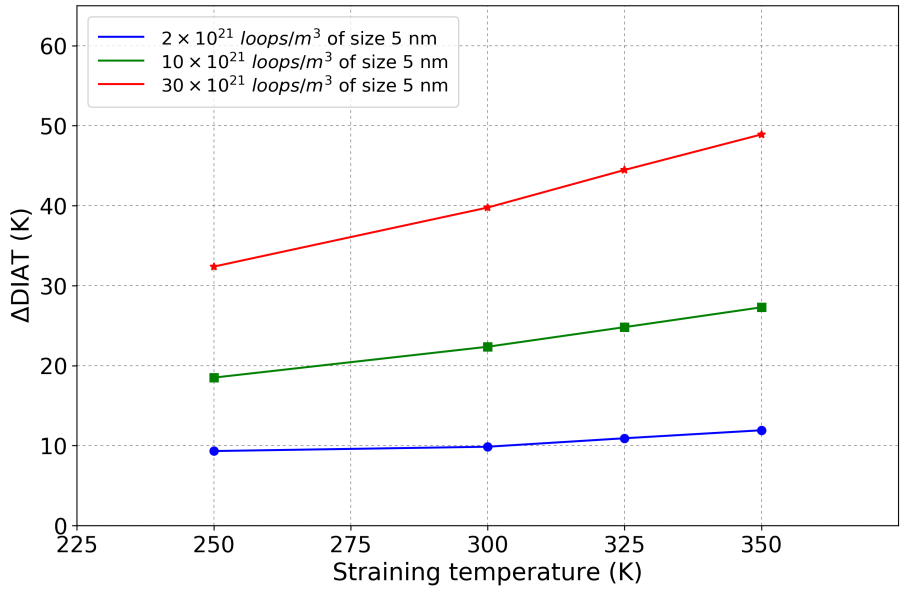

Figure 11: Numerically predicted ΔDIAT due to irradiation ($T_{irr} > 70^{\circ}C$) for 0.002 dpa (2×10^{21} $loops/m^3$), 0.01 dpa (10×10^{21} $loops/m^3$) and 0.15 dpa (30×10^{21} $loops/m^3$)

7 Discussion

The numerically predicted defect induced hardening is shown in Fig. 12a. The hardening effect is more pronounced above 150 K and increases with the straining temperature. The comparison of the non-irradiation and irradiation cases in terms of τ_{LT} and τ_{self} is shown in Fig. 12b. In the irradiated case, the temperature dependent increase of τ_{LT} is larger as compared to τ_{self}. This highlights the dominance of defect-induced hardening as compared to forest dislocations hardening.

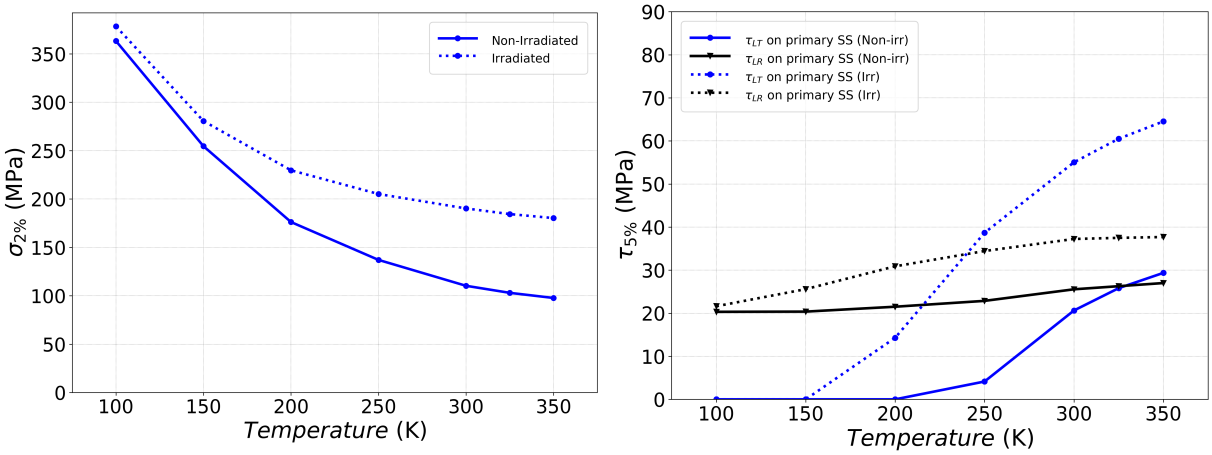

(a) (b)

Figure 12: a) Hardening effect of irradiation in terms of the shift in stress at 2% strain (2×10^{21} $loops/m^3$ of size 5nm) b) Critical shear stress components variation for the non-irradiated and irradiated case as a function of temperature

In non-irradiated case (Fig. 13a), the participation of secondary slip systems increases from straining temperature of 100 K ($\varepsilon_{sss}/\varepsilon_{pss} = 0.38$) to 250 K ($\varepsilon_{sss}/\varepsilon_{pss} = 0.67$), ε_{sss} is a strain on secondary slip system. Above this temperature, the contribution of secondary slip systems starts decreasing. In the presence of defect dispersion, however (Fig. 13a) the contribution of secondary slip systems is significant at low temperature only (below 150 K) where $\varepsilon_{sss}/\varepsilon_{pss} = 0.31$ at 150 K. The ratio $\varepsilon_{sss}/\varepsilon_{pss}$ as a function of temperature is shown in Fig. 13b. Recent DD simulation results have shown that defect-induced suppression of the secondary slip systems contribution is an indication of plastic strain localization [30, 73].

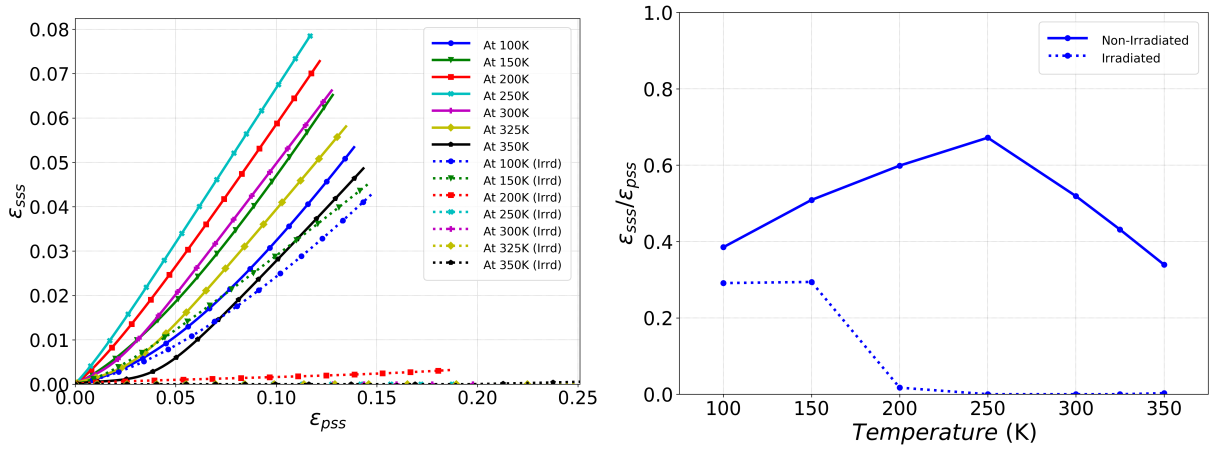

(a) (b)

Figure 13: Comparison between the non-irradiated and irradiated case for a) Strain of secondary slip system vs. strain on primary slip system b) ratio of strain on secondary slip system to strain on primary slip system vs. temperature

For nuclear reactor pressure vessel (RPV) steels, depending upon the material composition and irradiation conditions the value of DBTT shift reported ranges from 10 °C for *Fe-Cr* ferritic steels under fast neutron fluence of 2.2×10^{23} n/m^2 (at 300 °C) to 150 °C for higher dpa levels [1, 2, 53, 54, 60, 74]. The current model predicted the dependency of straining temperature and dose on ΔDIAT value, which is in-line with the dependency of DBTT on these parameters. It is worth mentioning that the presence of alloying elements may increase the value of shift in ΔDIAT significantly [75]. The alloying elements im-

part hindrance to the movement of dislocations depending upon their strength, size and number density. In addition, solute atom migration and subsequent segregation at brittle fracture initiating sites (particles, grain boundaries) also impact the DBTT value at a higher irradiation level. The current model has the capacity to account for alloying elements/carbides effect by treating them as obstacles to dislocation motion based on their number density and strength. However, it calls for extensive lower-scale studies (like molecular dynamics and DD) to establish the material parameters based on their interaction with dislocations before implementing them in the present crystal plasticity model.

The general trend for variation of various variables (τ_{eff}, τ_c, v, etc.) with respect to strain and temperature for the irradiated case along with ΔDIAT variation with straining temperature is in-line with the results of DD simulations, for a given defect dispersion case [32].

8 Summary

The proposed material model is based on dislocation mobility rules accounting for the thermally activated emission of kink pairs at low temperatures and athermal viscous drag flow at higher temperatures (up to 400 K). The dependence of screw dislocation velocity on its length allows for describing the effect of various dispersed obstacles (forest dislocations as obstacles, irradiation defects, particles, etc.) on the effective dislocation mobility. In the current formulation, dislocation density evolution based on storage and annihilation of dislocations is implemented. This allows estimating the defect-induced effects for various material conditions. The numerically predicted results are compared with experimental results available for pure-iron crystal and found to be in good agreement for temperature ranging from 15 K to 400 K.

The irradiation defects are accounted as obstacles to the dislocation motion, and the material model can predict the dose-dependent hardening satisfactorily in the BCC materials. The rate of change of irradiation defect cluster density (ρ_{irr}) is expressed as a function of strain rate. The generation of new dislocation sources due to the interaction of irradiation defects with dislocations is incorporated. The significant contribution of the secondary slip systems participation in the non-irradiated case and the presence of strain localization in the irradiated case is well predicted numerically.

The contribution of irradiation defects in the DBTT shift is estimated in terms of the ΔDIAT based on the relative change in the dislocation velocity field due to the presence of these defects. The ΔDIAT shift is estimated for different irradiation defect cluster densities within a straining temperature range of 250 K to 350 K.

Acknowledgments

The present research work was jointly supported by Indira Gandhi Centre for Atomic Research-DAE, India and Jules Horowitz Reactor-CEA, France. We wish to thank Vincent Ludovic and Helfer Thomas for their kind help and technical support during this work.

REFERENCES

[1] T. Lechtenberg, "Irradiation effects in ferritic steels," *Journal of Nuclear Materials*, vol. 133-134, pp. 149–155, 1985.

[2] P. Dubuisson, D. Gilbon, and J. Séran, "Microstructural evolution of ferritic-martensitic steels irradiated in the fast breeder reactor Phénix," *Journal of Nuclear Materials*, vol. 205, pp. 178–189, 1993.

[3] "Structural Materials for Liquid Metal Cooled Fast Reactor Fuel Assemblies-Operational Behaviour," *IAEA Nuclear Energy Series*, no. NF-T-4.3, 2012.

[4] T. Jayakumar, M. Mathews, and K. Laha, "High Temperature Materials for Nuclear Fast Fission and Fusion Reactors and Advanced Fossil Power Plants," *Procedia Engineering*, vol. 55, pp. 259–270, 2013.

[5] R. Klueh and A. Nelson, "Ferritic/Martensitic steels for next-generation reactors," *Journal of Nuclear Materials*, vol. 371, pp. 37–52, 2007.

[6] F. Roters, P. Eisenlohr, T. R. Bieler, and D. Raabe, *Crystal Plasticity Finite Element Methods in Materials Science and Engineering*. Verlag GmbH and Co. KGaA, Weinheim: WILEY-VCH, 2010.

[7] F. Roters, P. Eisenlohr, L. Hantcherli, D. Tjahjanto, T. Bieler, and D. Raabe, "Overview of constitutive laws, kinematics, homogenization and multiscale methods in crystal plasticity finite-element modelling: Theory, experiments, applications," *Acta Materialia*, vol. 58, pp. 1152–1211, 2010.

[8] G. Taylor, "The Mechanism of Plastic Deformation of Crystals. Part I.-Theoretical.," *Proc. of the Royal Society of Landon. Series A, Containing Papers of Mathematical and Physical Character*, vol. 145, pp. 362–387, 1934.

[9] G. Taylor, "The Mechanism of Plastic Deformation of Crystals. Part II.-Comparison with Observations.," *Proc. of the Royal Society of Landon. Series A, Containing Papers of Mathematical and Physical Character*, vol. 145, pp. 388–404, 1934.

[10] D. Hull and D. Bacon, *Introduction to Dislocations*. Linacre House, Jordan Hill, Oxford: Butterworth-Heinemann, Fourth edition 2001.

[11] N. Balasubramanian, "The temperature dependence of the dislocation velocity-stress exponent," *Scripta Metallurgica*, vol. 3, pp. 21–24, 1969.

[12] G. J. Voyiadjis and F. H. Abed, "Microstructural based models for bcc and fcc metals with temperature and strain rate dependence," *Mechanics of Materials*, vol. 37(2), pp. 355–378, 2005.

[13] D. Cereceda, M. Diehl, F. Roters, D. Raabe, J. M. Perlado, and J. Marian, "Unraveling the temperature dependence of the yield strength in single-crystal tungsten using atomistically-informed crystal plasticity calculations," *International Journal of Plasticity*, vol. 78, pp. 242–265, 2016.

[14] L. Kubin, B. Devincre, and M. Tang, "Mesoscopic modelling and simulation of plasticity in fcc and bcc crystals: Dislocation intersections and mobility," *Journal of Computer-Aided Materials Design*, vol. 5, pp. 31–54, 1998.

[15] F. J. Zerilli and R. W. Armstrong, "Dislocation mechanics based constitutive relations for material dynamics calculations," *Journal of Applied Physics*, vol. 61, pp. 1816–1825, 1987.

[16] R. Armstrong and F. Zerilli, "Dislocation mechanics based analysis of material dynamics behavior," *Journal de Physique Colloques*, vol. 49, pp. C3–529–C3–534, 1988.

[17] L. Stainier, A. Cuitino, and M. Ortiz, "A micromechanical model of hardening, rate sensitivity and thermal softening in bcc single crystals," *Journal of Mechanics and Physics of Solids*, vol. 50, pp. 1511–1545, 2002.

[18] A. Ma, F. Roters, and D. Raabe, "Studying the effect of grain boundaries in dislocation density based crystal-plasticity finite element simulation," *International Journal of Solids and Structures*, vol. 43, pp. 7287–7303, 2006.

[19] A. Alankar, P. Eisenlohr, and D. Raabe, "A dislocation density-based crystal plasticity constitutive model for prismatic slip in α -titanium," *Acta Materialia*, vol. 59, pp. 7003–7009, 2011.

[20] G. Monnet, S. Naamane, and B. Devincre, "Orowan strengthening at low temperature in bcc materials studied by dislocation dynamics," *Acta Materialia*, vol. 59, pp. 451–461, 2011.

[21] T. H. Blewitt, R. Coltman, R. Jamison, and J. Redman, "Radiation hardening of copper single crystals," *Journal of Nuclear Materials 2*, vol. 4, pp. 277–298, 1960.

[22] G. Lucas, "The evolution of mechanical property change in irradiated austenitic stainless steels," *Journal of Nuclear Materials*, vol. 206, pp. 287–305, 1993.

[23] B. Singh, A. Foreman, and H. Trinkaus, "Radiation hardening revisited: role of intracascade clustering," *Journal of Nuclear Materials*, vol. 249, pp. 103–115, 1997.

[24] A. Arsenlis, B. Wirth, and M. Rhee, "Dislocation density-based constitutive model for the mechanical behaviour of irradiated cu," *Philosophical Magazine*, vol. 84, pp. 3617–3635, 2004.

[25] M. Tang, L. Kubin, and G. Canova, "Dislocation mobility and the mechanical response of b.c.c. single crystals: A mesoscopic approach," *Acta Materialia*, vol. 46, pp. 3221–3235, 1998.

[26] D. Cedat, O. Fandeur, C. Rey, and D. Raabe, "Polycrystal model of the mechanical behavior of a $Mo-TiC_{30\ vol.\%}$ metal-ceramic composite using a three-dimensional microstructure map obtained by dual beam focused ion beam scanning electron microscopy," *Acta Materialia*, vol. 60, pp. 1623–1632, 2012.

[27] U. Kocks, A. Argon, and M. Ashby, "Thermodynamics and kinetics of slip," *Pergamon Press*, vol. 19, p. 291, 1975.

[28] S. Naamane, G. Monnet, and B. Devincre, "Low temperature deformation in iron studied with dislocation dynamics simulation," *International Journal of Plasticity*, vol. 26, pp. 84–92, 2010.

[29] G. Monnet, L. Vincent, and B. Devincre, "Dislocation-dynamics based crystal plasticity law for the low- and high-temperature deformation regimes," *Acta Materialia*, vol. 61, pp. 6178–6190, 2013.

[30] K. Gururaj, C. Robertson, and M. Fivel, "Post-irradiation plastic deformation in bcc fe grains investigated by means of 3d dislocation simulations," *Journal of Nuclear Materials*, vol. 459, pp. 194–204, 2015.

[31] Y. Estrin and H. Mecking, "A unified phenomenological description of work hardening and creep based on one-parameter model," *Acta Metallurgica*, vol. 32, pp. 57–70, 1984.

[32] Y. Li and C. Robertson, "Irradiation defect dispersions and effective dislocation mobility in strained ferritic grains: A statistical analysis based on 3D dislocation dynamics simulation," *Journal of Nuclear Materials*, vol. 504, pp. 84–93, 2018.

[33] D. Caillard, "Kinetics of dislocations in pure fe. part i. in situ straining experiments at room temperature," *Acta Materialia*, vol. 58, pp. 3493–3503, 2010.

[34] A. Stukowski, D. Cereceda, T. D. Swinburne, and J. Martian, "Thermally-activated non-Schmid glide of screw dislocations in W using atomistically-informed kinetic Monte Carlo simulations," *International Journal of Plasticity*, vol. 65, pp. 108–130, 2015.

[35] F. Louchet and L. Kubin, "Dislocation substructure in the anomalous slip plane of single crystal niobium strained at 50 k," *Acta Matallurgica*, vol. 23, pp. 17–21, 1975.

[36] M. Tang, B. Devincre, and L. Kubin, "Simulation and modelling of forest hardening in body center cubic crystals at low temperature," *Modelling and Simulation in Materials Science and Engineering*, vol. 7, pp. 893–908, 1999.

[37] T. Cadman and R. Arsenault, "The nature of dislocation motion through a random array of thermally activatable obstacles," *Scripta Metallurgica*, vol. 6, pp. 593–600, 1972.

[38] W. Spitzig, "The effect of orientation, temperature and strain rate on deformation of Fe-0.16 w.% Ti single crystals," *Material Science and Engineering*, vol. 12, pp. 191–202, 1973.

[39] D. Quesnel, A. Sato, and M. Meshii, "Solution softening and hardening in the iron-carbon system," *Material Science and Engineering*, vol. 18, pp. 199–208, 1975.

[40] E. Kuramoto, Y. Aono, and K. Kitajima, "Thermally activated slip deformation of high purity iron single crystals between 4.2 k and 300 k," *Scripta Metallurgica*, vol. 13, pp. 1039–1042, 1979.

[41] J. P. Hirth and J. Lothe, *Theory of Dislocations*. Malabar, Florida: Krieger Publishing Company, Second Edition, 1982.

[42] P. Franciosi, M. Berveiller, and A. Zaoui, "Latent hardening in copper and aluminium single crystals," *Acta Metallurgica*, vol. 28, pp. 273–283, 1980.

[43] D. Peirce, R. Asaro, and A. Needleman, "An Analysis of Nonuniform and Localized Deformation in Ductile Single Crystals," *Division of Engineering, Brown University, Providence. RI 02912. U.S.A.*, 1981.

[44] B. Devincre, L. Kubin, and T. Hoc, "Physical analyses of crystal plasticity by dd simulations," *Scripta Materialia*, vol. 54, pp. 741–746, 2006.

[45] B. Devincre, T. Hoc, and L. P. Kubin, "Collinear interaction of dislocation and slip systems," *Materials Science and Engineering A*, vol. 400-401, pp. 182–185, 2005.

[46] R. Madec, B. Devicre, L. Kubin, T. Hoc, and D. Rodney, "The role of collinear interaction in dislocation-induced hardening," *Science Magazine*, vol. 301, pp. 1879–1882, 2003.

[47] M. Khadyko, S. Dumoulin, and O. S. Hopperstad, "Slip system interaction matrix and its influence on the macroscopic response of Al alloys," *Materials Science Forum*, vol. 794-796, pp. 566–571, 2014.

[48] A. Siddiq and S. Schmauder, "Crystal plasticity parameter identification procedure for single crystalline material during deformation," *Journal of Computational and Applied Mechanics*, vol. 7, pp. 1–15, 2006.

[49] R. Madec and L. Kubin, "Dislocation interaction and symmetries in BCC crystals," *IUTAM Symposium on Mesoscopic Dynamics of Fracture Process and Materials Strength*, pp. 69–78, 2004.

[50] S. Queyreau, G. Monnet, and B. Devincre, "Slip system interaction in alpha iron determined by dislocation dynamics simulations," *International Journal of Plasticity*, vol. 25, pp. 361–377, 2009.

[51] U. Kocks and H. Mecking, "Physics and phenomenology of strain hardening: the fcc case," *Progress in Materials Sciences*, vol. 348, pp. 171–273, 2003.

[52] B. Devincre, T. Hoc, and L. Kubin, "Dislocation mean free paths and strain hardening of crystals," *Science (Reports)*, vol. 320, pp. 1745–1748, 2008.

[53] H. Kayano, A. Kimura, M. Narui, Y. Sasaki, Y. Suzuki, and S. Ohta, "Irradiation embrittlement neutron-irradiated low activation ferritic steels," *Journal of Nuclear Materials*, vol. 155-157, pp. 978–981, 1988.

[54] D. S. Billington and J. James H. Crawford, *Radiation damage in solids*. Princeton, New Jersey: Princeton university press, 1961.

[55] D. Terentyev, D. Bacon, and Y. Osetsky, "Reaction between a $1/2\langle 111\rangle$ screw dislocation and $\langle 100\rangle$ interstitial dislocation loops in alpha-iron modelled at atomic scale," *Philosophical magazine*, vol. 90, pp. 1019–1033, 2010.

[56] D. Terentyev, P. Grammatikopoulos, D. Bacon, and Y. Osetsky, "Simulation of the interaction between an edge dislocation and $\langle 100\rangle$ interstitial dislocation loop in α - iron," *Acta Materialia*, vol. 56, pp. 5034–5046, 2008.

[57] M. Jenkins, Z. Yao, M. HernÃ ndez-Mayoral, and M. Kirk, "Dynamics observations of heavy-ion damage in fe and fe-cr alloys," *Journal of Nuclear Materials*, vol. 389, pp. 197–202, 2009.

[58] C. Robertson and M. Fivel, "Dislocation/defect interaction in alpha-fe grain under post-irradiation plastic straining: a 3d dislocation dynamics investigation," Deliverable D1-2.2 7th Euratom project PERFORM 60, CEA, CNRS, 2013.

[59] M. Tanaka, E. Tarleton, and S. Roberts, "The brittle-ductile transition in single-crystal iron," *Acta Materialia*, vol. 56, pp. 5123–5129, 2008.

[60] J. Koutsky and J. Kocik, "Radiation damage of structural materials," *Material Science Monograph*, vol. 79, 1994.

[61] T. Swinburne and S. Dudarev, "Kink-limited orowan strengthening explains the brittle t ductile transition of irradiated and un-irradiated bcc materials," *Physical Review Materials*, vol. 2, p. 073608, 2018.

[62] H. Thomas, M. Bruno, P. Jean-Michel, S. Maxime, S. Jerome, and C. Michel, "Introducing the open-source mfront code generator: Application to mechanical behaviours and material knowledge management within the PLEIADES fuel element modelling platform.," *Computers & Mathematics with Applications*, vol. 70, pp. 994–1023, 2015.

[63] A. Cuitino and M. Ortiz, "Computational modelling of single crystals," *Modelling and Simulation in Materials Science and Engineering I*, pp. 225–263, 1992.

[64] N. Jia, P. Eisenlohr, D. Roters, and X. Zhao, "Orientation dependence of shear banding in face-centred-cubic single crystals," *Acta Materialia*, vol. 60, pp. 3415–3434, 2012.

[65] X. Xiazi, "Fundamental Mechanisms for Irradiation-Hardening and Embrittlement: A Review," *Metals*, vol. 9, no. 10, 2019.

[66] M. Briceno, J. Kacher, and I. Robertson, "Dynamics of dislocation interactions with stacking-fault tetrahedra at high temperature," *Journal of Nuclear Materials*, vol. 433, no. 1, pp. 390 – 396, 2013.

[67] B. Singh, N. Ghoniem, and H. Trinkaus, "Experiment-based modelling of hardening and localized plasticity in metals irradiated under cascade damage conditions," *Journal of nuclear materials*, vol. 307, pp. 159–170, 2002.

[68] T. D. de la Rubia, H. M. Zbib, T. A. Khraishi, B. D. Wirth, M. Victoria, and M. J. Caturla, "Multiscale modelling of plastic flow localization in irradiated materials," *Nature*, vol. 406, pp. 871–874, 2000.

[69] O. Chopra and A. Rao, "A review of irradiation effects on LWR core internal materials-neutron embrittlement," *Journal of nuclear materials*, vol. 412, pp. 195–208, 2011.

[70] Z. YAO, *The relationship between the irradiation induced damage and the mechanical properties of single crystal Ni*. PhD thesis, Ecole polytechnique federale de lausanne, 2005.

[71] M. Eldrup, B. Singh, S. Zinkle, T. Byun, and K. Farrell, "Dose dependence of defect accumulation in neutron irradiation copper and iron," *Journal of Nuclear Materials*, vol. 307-311, pp. 912–917, 2002.

[72] S. Zinkle and B. Singh, "Microstructure of neutron-irradiated iron before and after tensile deformation," *Journal of Nuclear Materials*, vol. 351, pp. 269–284, 2006.

[73] A. Arsenlis, M. Rhee, G. Hommes, R. Cook, and J. Marian, "A dislocation dynamics study of the transition from homogeneous to heterogeneous deformation in irradiated body-centered cubic iron," *Acta Materialia*, vol. 60, pp. 3748–3757, 2012.

[74] R. Stoller, "The effect of neutron flux on radiation-induced embrittlement in reactor pressure vessel steels," *Journal of ASTM International*, vol. STP 1447, pp. 326–337, 2004.

[75] Y. Nikolaev, A. Nikolaev, and Y. Shtrombakh, "Radiation embrittlement of low-alloy steels," *International journal of pressure vessel and piping*, vol. 79, pp. 619–636, 2002.